Degradation of Poly(ethylene glycol) by Electrolysis During the Cu Electroplating: A Combined Experimental and Density Functional Theory Study

Yong Sun Won, Donghyun Cho, Yunhee Kim, Jinuk Lee, Sung Soo Park

Samsung Electro-Mechanics Co. Ltd., Corporate R&D Institute, Suwon, Gyunggi-Do 443-743, Korea

Received 13 January 2009; accepted 17 June 2009
DOI 10.1002/app.31025
Published online 7 April 2010 in Wiley InterScience (www.interscience.wiley.com).

ABSTRACT: The polymer additives are key factor materials in the Cu electroplating process, essential for controlled acceleration and inhibition of Cu deposition. In this study, the degradation behavior of a polymer additive—poly(ethylene glycol) (PEG)—during the Cu electroplating was investigated by MALDI-TOF MS technique. The PEG was completely degraded after 4 h at a constant electric current density of 13 mA/cm^2, whereas it showed no degradation without an electric field even at a very low pH (pH $<$ 1). The pathways and energetics of PEG degradation by electrolysis in aqueous chloride medium was investigated using density functional theory calculations at the same time. It demonstrated how facile the decomposition of PEG internal radical is, which is generated via the hydrogen abstraction from PEG by hydroxyl radical formed at the anode in aqueous chloride medium under an electric field. © 2010 Wiley Periodicals, Inc. J Appl Polym Sci 117: 2083–2089, 2010

Key words: MALDI-TOF MS; PEG degradation; Cu electroplating; DFT calculation

INTRODUCTION

The polymer additives play important roles in the Cu electroplating process.[1–8] Although many aspects of the functions of polymer additives have been known, the interest has continued on obtaining an improved fundamental understanding of their behavior as the plating suppressor.[9] The water-soluble polymers such as poly(ethylene glycol) (PEG) and poly(propylene glycol) have been widely used as the carrier in the Cu electroplating. The carrier suppresses copper plating mildly by forming a stable diffusion layer at the cathode. However, the polymer additives are easily degraded by an applied electric current density and air bubbling during the Cu electroplating.

It is known that the PEG is less stable than pure hydrocarbon polymer such as polyethylene or polypropylene, because C—O bond is less stable than C—C counterpart.[10,11] The mechanism of PEG degradation was often explained by complex free-radical and oxidative reactions accompanied by main C—O bond scission.[10–12] It was reported that the hydroxyl radical (•OH) produced from H_2O_2 abstracts hydrogen from a methyl group in PEG to generate PEG internal radical (**IR**) and H_2O, and the free radical is then decomposed by C—O homolysis.[13] A similar free radical decomposition scheme was confirmed for water-soluble polymers by irradiation in the presence of O_2.[14]

There exist no explicit oxidation agents (H_2O_2 or irradiation in the presence of O_2) in the Cu electroplating. Chen and Rajeshwar, however, reported that the hypochlorite ion (OCl^-) is generated by electrolysis at the anode in aqueous chloride medium[15,16] as follows:

$$2Cl^- \rightarrow Cl_2 + 2e^- \quad (1)$$

$$Cl_2 + H_2O \leftrightarrow HOCl + Cl^- + H^+ \quad (2)$$

$$HOCl \leftrightarrow H^+ + OCl^- \quad (3)$$

$$6OCl^- + 3H_2O \rightarrow 2O_3Cl^- + 4Cl^- + 6H^+ + 3/2O_2 + 6e^- \quad (4)$$

$$O_3Cl^- + H_2O \rightarrow 2O_4Cl^- + 2H^+ + 2e^- \quad (5)$$

$$OCl^- + 2HOCl \rightarrow ClO_3{}^- + 2Cl^- + 2H^+ \quad (6)$$

Fukatsu and Kokot[17] found that the degradability of PEG is proportional to the chlorine ion concentration, confirming hypochlorite ions (OCl^-) contributed to produce hydroxyl radicals, which are capable of abstracting hydrogen from PEG. The mechanism for the hydroxyl radical formation had been suggested by Khatua and Hsieh[18] in their study of the chlorine degradation of polyether-based polyurethane, as presented in reactions 7–9. Epstein

Correspondence to: Y. S. Won (yongsun.won@samsung.com).

and Lewin[19] reported that the reaction rate of the oxidation of cellulose fibers in an aqueous hypochlorite solution is proportional to the concentration of HOCl square and to the square root of the concentration of OCl^-. It is also known that the degradation of polymer carriers in the Cu electroplating is higher at the anode (Technical information provided by ATOTECH), where the hypochlorite ions are generated, and the degradation is reduced when anodes are filmed or bagged.

$$HOCl + OCl^- \rightarrow ClO\bullet + Cl^- + OH\bullet \quad (7)$$

$$OH\bullet + OCl^- \rightarrow ClO\bullet + OH^- \quad (8)$$

$$OCl\bullet + OCl^- + OH^- \rightarrow 2Cl^- + O_2 + OH\bullet \quad (9)$$

In this study, the degradation of PEG by electrolysis during the Cu electroplating is investigated in a combined approach of matrix-assisted laser desorption ionization time-of-flight mass spectrometry (MALDI-TOF MS) experiments and computational analyzes based on density functional theory (DFT) calculations. The MALDI-TOF MS technique is ideal for the detailed structural analysis of synthetic polymer additives among other various characterization methods of polymers.[12,20–22] MALDI is a soft ionization technique used in MS, allowing the analysis of large organic molecules such as biomolecules and polymers, which are fragile to be easily fragmented when ionized by a laser beam (normally a nitrogen laser). A matrix is used to protect the organic molecules from being destroyed by direct laser beam.

EXPERIMENTAL

Chemicals

The PEG, named PEG 4000, was obtained from Polymer Standards Service (SDKC-400). The sample was prepared for MALDI-TOF MS experiments using the following matrix and cationization agent: 2, 4, 6-trihydroxy acetophenone (THAP) and sodium trifluoro-acetate (NaTFA), both were obtained from Aldrich and dissolved in methanol (Adrich, HPLC grade) at a concentration of 10 mg/mL.

Sample solution preparation

The Cu electroplating solution for experiments was prepared according to the protocol used for the real Cu electroplating process. The details are not presented here. For the characterization of PEG 4000 under an excess of the cupric and sulfate ions, the sample pretreatment is highly required. For this purpose, the chemical precipitation was introduced at the sample preparation step. To remove the cupric and sulfate ions, 17.5 mL of NaOH 1.0*M* solution was added to 10 mL of the Cu electroplating solution. On the completion of precipitation, the supernatant of the Cu electroplating solution was applied for MALDI-TOF analysis.

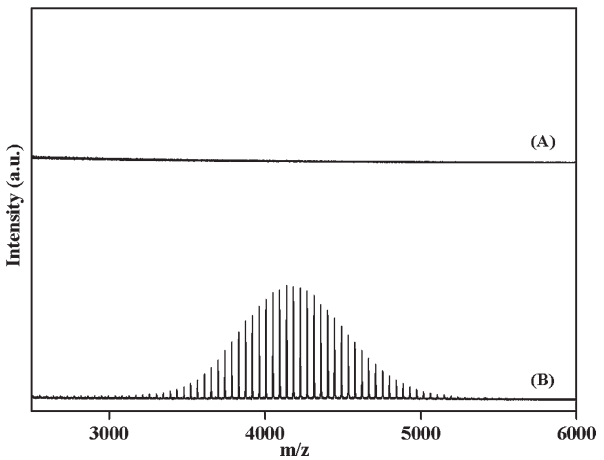

Figure 1 MALDI-TOF mass spectra of PEG 4000 dissolved in Cu electroplating solution before (A) and after (B) chemical precipitation treatment of the solution.

MALDI-TOF MS

In MALDI-TOF MS experiments, a Bruker Autoflex II mass spectrometer was used. The spectrometer is equipped with a nitrogen laser (λ = 337 nm), a pulsed ion extraction (PIE), and a reflector. The ions were extracted from the source with an acceleration voltage of +19 kV and detected by a microchannel plate. Mass spectra were recorded at a laser power set slightly above the ionization threshold to avoid fragmentation and to maximize the resolution. The operating conditions of the mass spectrometer were as follows: ion source 1 = 19 kV, ion source 2 = 16.85 kV, lens voltage = 8.50 kV, reflector voltage = 20.00 kV, optimized PIE time = 160 ns, matrix suppression = 860 Da, detector gain = 7.1, and positive reflection mode. Spectra were collected by moving the laser around the surface of the sample to yield high analyte signals. Samples for MALDI-TOF analysis were prepared by mixing THAP (2.5 mg/100 mL in methanol), analyte solution (Cu plating solution including polymer additives), and NaTFA (2 mg/100 mL in methanol) in a volume ratio of 100 : 100 : 3, respectively. About 0.5 mL of the appropriate mixture solution was spotted on the sample plate (MTP 384 target ground steel TF) and allowed to air-dry under ambient condition.

Computational details

All calculations were carried out with GAUSSIAN 03 program package, using B3LYP (Becke, three-parameter, Lee-Yang-Parr) hybrid exchange DFT model chemistry and 6-31G(d,p) basis set.[23–25] Full geometry optimization was carried out for all species.

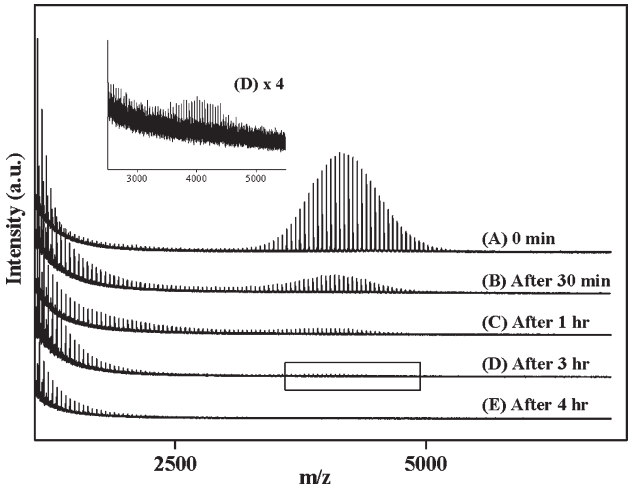

Figure 2 MALDI-TOF mass spectra of PEG 4000 dissolved in Cu electroplating solution, demonstrating the effect of the plating time on the polymer degradation at constant electric current; no electric field (A), after exposure to a constant electric current density (13 mA/cm^2) for 30 min (B), 1 h (C), 3 h (D), 4 h (E). The insert represents the expanded region ($\times$4) of (D) in the range of m/z 2500 $\sim$ 5500 Da.

Harmonic vibration frequencies were calculated for all optimized structures to allow classification of the various structures as minima or transition states, and used to compute Gibbs energies. Material Studio 4.2 was used for the visualization of the results.

RESULTS AND DISCUSSION

MALDI-TOF analysis

In the first set of experiments, the MALDI-TOF analysis of PEG 4000 with an excess of cupric and sulfate ions was compared with the result after the removal of cupric and sulfate ions from the Cu electroplating solution by chemical precipitation. Figure 1 shows MALDI-TOF mass spectra of PEG 4000 before (A) and after (B) the pretreatment of the Cu electroplating solution. From the Figure 1(A), we found that the excess amount of cupric and sulfate ions prevents obtaining MALDI-TOF mass spectrum of PEG 4000. In this severe condition, we could not obtain

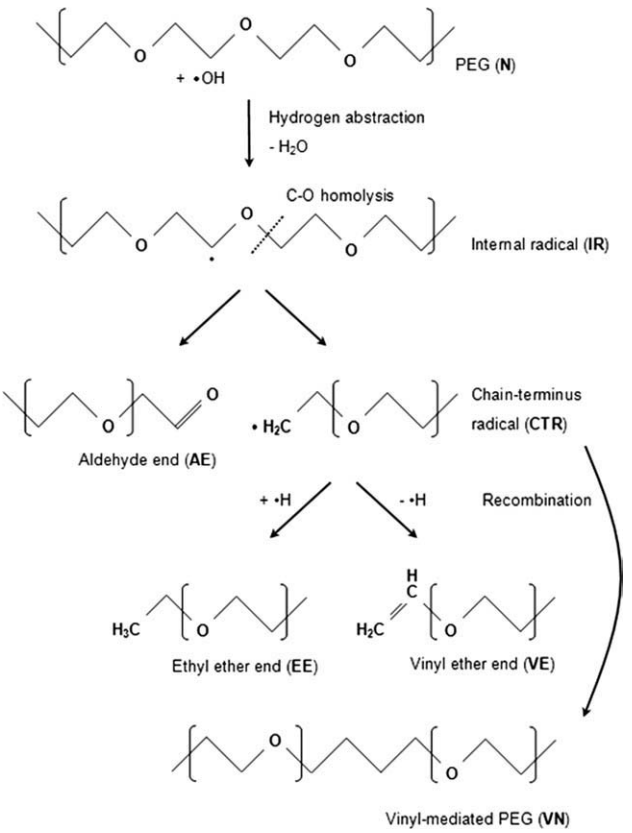

Scheme 1 PEG decomposition pathways by electrolysis.

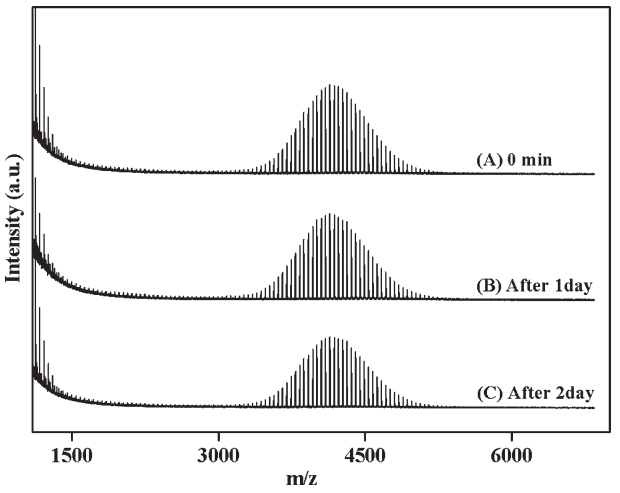

Figure 3 MALDI-TOF mass spectra of PEG 4000 dissolved in Cu electroplating solution without exposure to the electric field for 1 (A), 2 (B), and 3 days (C).

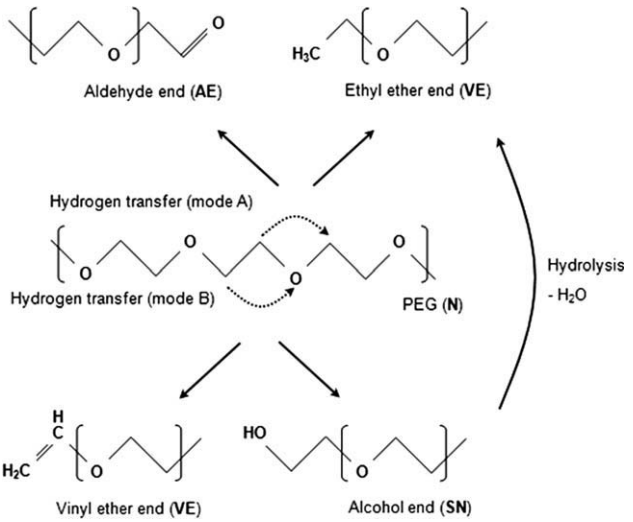

Scheme 2 PGE thermal decomposition pathways.

TABLE I
Structures of the Principal Fragments of PEG Decomposition

N	Normal (dihydroxyl). HO—(—C_2H_4—O—)$_n$—H
IR	Internal radical. HO—(—CH_2—•CH—O—)$_n$—H
CTR	Chain-terminus radical. •CH_2—CH_2—O—(—C_2H_4—O—)$_n$—H
AE	Aldehyde. HCO—CH_2—O—(—C_2H_4—O—)$_n$—H
VE	Vinyl ether. CH_2=CH—O—(—C_2H_4—O—)$_n$—H
EE	Ethyl ether. C_2H_5—O—(—C_2H_4—O—)$_n$—H
VN	Vinyl-mediated PEG H—(—O—C_2H_4—)$_n$—O—CH_2—CH_2—CH_2—CH_2—O—(—C_2H_4—O—)$_n$—H
SN	Alcohol. HO—(—C_2H_4—O—)$_n$—H

any mass spectrum of polymer additives. In contrast, removing the cupric and sulfate ions by chemical precipitation led to a high-quality MALDI-TOF mass spectrum as shown in Figure 1(B). From this, we concluded that the sample pretreatment is essential for the MALDI-TOF analysis of polymer additives in Cu electroplating solution.

Electric current effect on the degradation of polymer additives

In this section, the degradation behavior of PEG 4000 regarding the electric current density was carefully investigated. Figure 2 shows the time-dependent mass spectra of PEG 4000 recorded at an electric current density of 13 mA/cm^2, adjusted to the value used in the real Cu electroplating process. In all cases, the cupric and sulfate ions were completely removed by the pretreatment of chemical precipitation for MALDI-TOF measurement. Figure 2(A) shows the mass spectrum of PEG 4000 with no electric field. As the plating time passes, the MALDI-TOF mass spectrum of PEG 4000 is dramatically changed as shown in Figure 2(B–E). We found that all high molecular weight (MW) species of PEG 4000 were completely degraded and the peaks were shifted to the low MW region after 4 h. It implies that the polymer additive loses its capacity as a plating suppressor for the Cu electroplating after 4 h and thus the polymer additive must be supplied continuously to control the Cu plating rate and surface roughness stably.

Meanwhile, there was no effect of pH on the degradation of PEG 4000 without an electric field. The pH of the Cu electroplating solution is very low (pH < 1), providing a highly acidic condition. The pH effect on polymer additives was, thus, also examined. Figure 3 shows the MALDI-TOF mass spectra of PEG 4000 with respect to the time interval at a very low pH (pH < 1). From the figure, it is concluded that the degradation rate of PEG 4000 is very slow and the effect of pH on the degradation of polymer additives is negligible.

Computational study on the degradation of poly(ethylene glycol) by electrolysis in aqueous chloride medium

Based on the results in the literature,[10–12] the decomposition pathways of PEG **IR** are proposed in the Scheme 1. As previously mentioned, the hypochlorite ion (OCl^-)s are electrochemically formed at the anode during the Cu electroplating in an aqueous chloride medium [eqs. (1)–(6)], and contribute to the formation of hydroxyl radicals [eqs. (7)–(9)]. The PEG **IR**s are then generated via the hydrogen abstraction from PEG by hydroxyl radicals. The Scheme 2 represents the thermal decomposition pathways of PEG for comparison.

Structures of the various PEG decomposition fragments are summarized in Table I. A PEG chain with $n = 5$ (see **N** in Fig. 4) and its **IR** (see **IR** in Fig. 4) were then selected as base species for the computational analysis. Computing capacity was considered for the selection. The geometry optimization and frequency calculation of each fragment were carried out to obtain the energetics of the Schemes 1 and 2.

A long PEG chain, in fact, experiences conformational change in aqueous solution. The gauche conformation around the C—C bond was reported to stabilize PEG chain by hydrogen bonding of water.[26,27] A similar conformational change was also observed in PEG-Cu-Cl complex, which plays a

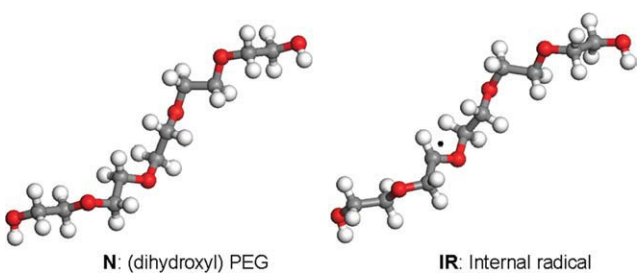

Figure 4 DFT-optimized geometries of PEG ($n = 5$) (**N**) and PEG internal radical (**IR**). [Color figure can be viewed in the online issue, which is available at www.interscience.wiley.com.]

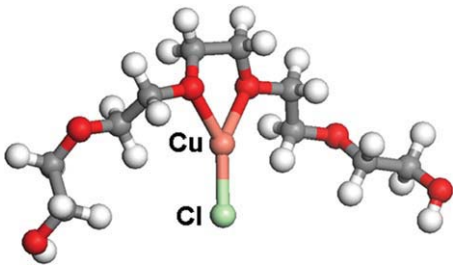

Figure 5 DFT-optimized geometry of PEG ($n = 5$)-Cu-Cl complex. [Color figure can be viewed in the online issue, which is available at www.interscience.wiley.com.]

significant role in PEG adsorption to the electrode surface in the Cu electroplating.[1] A PEG ($n = 5$)-Cu-Cl complex is shown in Figure 5, obtained by DFT geometry optimization. However, the energy build-up in the PEG chain by the conformational change was found to be small ($\Delta = +1.4$ kcal/mol) to be ignored.

The reaction energies for all the reactions described in the Schemes 1 and 2 were calculated by the following expression, and listed in Table II.

$$\Delta G^{\circ}_{\mathrm{rxn}} = \sum G^{\circ}(\mathrm{products}) - \sum G^{\circ}(\mathrm{reactants}) \quad (10)$$

$$\Delta G^{\circ}_{\mathrm{rxn}} = [G^{\circ}(\mathrm{C}) + G^{\circ}(\mathrm{D})] - [G^{\circ}(\mathrm{A}) + G^{\circ}(\mathrm{B})] \quad \text{for} \quad \mathrm{A} + \mathrm{B} \rightarrow \mathrm{C} + \mathrm{D}$$

In the presence of hydroxyl radical (•OH), the hydrogen abstraction from a methyl group in PEG (**N**) to produce a PEG **IR** was verified to be thermodynamically favorable (negative reaction energy). The effect of positive entropy generation (1 mol → 2 mol) favors the decomposition processes of the reactions 2 and 5–7 in general. For the reactions 3 and 4 to generate stable fragments (**EE**, **VE**, and **VN**) out of radical (**CTR**)s, the reaction energies are also highly negative. Therefore, kinetic constraints must be taken into account to evaluate if those reactions could really occur at the given condition, that is, at ~ 50°C typically used in the Cu electroplating. The transition states for the reactions of PEG decomposition were located as shown in Figure 6 and the activation energies were listed also in Table II, calculated similarly as follows:

$$\Delta G^{\circ}_{\mathrm{act}} = G^{\circ}(\text{transition state}) - \sum G^{\circ}(\text{reactants}) \quad (11)$$

$$\Delta G^{\circ}_{\mathrm{act}} = [G^{\circ}(\mathrm{AB}^{\ddagger})] - [G^{\circ}(\mathrm{A}) + G^{\circ}(\mathrm{B})] \quad \text{for} \quad \mathrm{A} + \mathrm{B} \rightarrow \mathrm{AB}^{\ddagger}$$

The reaction 1 comprises two steps; **N** + •OH → **N**···HO• → **IR** + H_2O. The hydrogen atom in hydroxyl radical (•OH) forms hydrogen bonding with one of the oxygen atoms in PEG (**N**) and the stabilized intermediate goes through the transition state (see Fig. 5) to generate PEG **IR** and water by hydrogen abstraction. The overall activation energy was calculated to be 3.2 kcal/mol (0.9 kcal/mol for forming the intermediate + 2.3 kcal/mol for hydrogen abstraction), which is very small to be overcome. In addition, the electro–chemical potential (Ψ_E) applied in the Cu electroplating lowers the net activation barrier ($\Delta G^{\circ}_{\mathrm{act}} - \Psi_E$) to drive the reaction more facile. The standard Cu reduction potential (E°) is 0.340 V for $Cu^{2+} + 2e^{-} \rightarrow$ Cu. Thus, the electro–chemical potential for Cu reduction (Ψ°_E) is 15.7 kcal/mol, simply calculated by the expression, $\Psi_E = \nu\, FE$. Here, ν is the net charge transferred (= 2), F is the Faraday constant (= 96,485 C/mol), and E is the potential difference (= 0.340 J/C). The actual electro–chemical potential (Ψ_E) applied for the Cu electroplating must be greater than this value. In the homolytic fission or fusion (in other words, simple bond dissociation or formation) like reactions 2 and 4, it was known that the activation energy is not much larger than—practically same as—the reaction energy.[28,29] It implies that the reactions 2 and 4 readily occur with their negative

TABLE II
Calculated Reaction and Activation Energies for the Reactions of PEG decomposition; Reactions 1–4 for the Scheme 1 and Reactions 5–7 for the Scheme 2

		Reactions	Reaction energy $\Delta G^{\circ}_{\mathrm{rxn}}$ (kcal/mol)	Activation energy $\Delta G^{\circ}_{\mathrm{act}}$ (kcal/mol)
Scheme 1	1	**N**+ •OH ↔ **IR**+ H_2O	−22.6	3.2
	2	**IR** ↔ **AE** + **CTR**	−4.8	−4.8
	3	**2CTR** ↔ **EE** + **VE**	−67.7	19.8
	4	**2CTR** ↔ **VN**	−70.1	−70.1
Scheme 2	5	**N** ↔ **AE** + **VE** (mode A)	−15.1	99.6
	6	**N** ↔ **VE** + **SN** (mode B)	−2.8	63.9
	7	**SN** ↔ **VE** + H_2O	−1.7	66.0

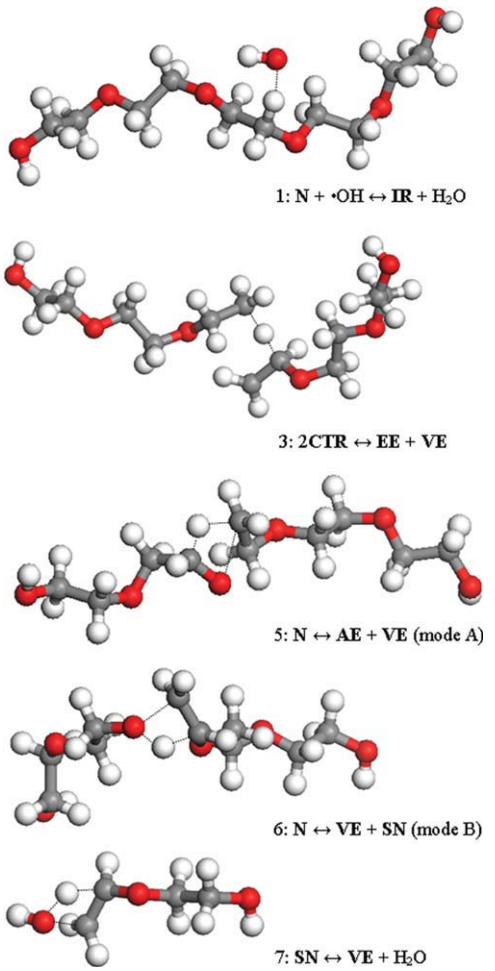

Figure 6 Transition states for the reactions of PEG decomposition. [Color figure can be viewed in the online issue, which is available at www.interscience.wiley.com.]

activation energies. The transition state for the reaction 3 was presented in Figure 5, in which a hydrogen atom is transferred from one chain-terminus radical (**CTR**) to leave behind a stable vinyl ether (**VE**) end fragment and produce a stable ethyl ether (**EE**) end fragment in the other **CTR**. The calculated activation energy of 19.8 kcal/mol is significant as a barrier. Although the applied electro–chemical potential (Ψ_E) could facilitate the reaction 3 by lowering the net activation barrier by $>$ 15.7 kcal/mol, the recombination of **CTR**s in the reaction 4 to produce vinyl-mediate PEG (**VN**) would be more favorable. The C═O bond in the aldehyde end fragment (**AE**) generated by the reaction 2, which has no further reaction steps unlike **CTR**, has thus been used as an experimental indicator for the C—O bond scission of **IR**.[17] Meanwhile, the activation barriers for the pure thermal decomposition of PEG (reactions 5–7 in the Scheme 2) were too significant to be simply overcome even under an electric field.

CONCLUSION

It was confirmed both experimentally and computationally that the PEG as an additive in the Cu electroplating was degraded by electrolysis. The MALDI-TOF analysis showed the complete degradation of PEG in the Cu electroplating solution after 4 h at a constant electric current density of 13 mA/cm^2, whereas there was no effect of the pH without an electric field. At the initial stage, hydroxyl radicals generated by hypochlorite ions at the anode in aqueous chlorine medium abstracts hydrogen atoms from a methyl group in PEG to produce PEG **IR**s. The C—O bond scission and complex radical decomposition follow. The DFT calculation was used to support the aforementioned mechanism of PEG degradation and demonstrate the facility of the formation and decomposition of PEG **IR** quantitatively, when compared with a corresponding thermal decomposition of PEG.

References

1. Feng, Z. V.; Li, X.; Gewirth, A. A. J Phys Chem B 2003, 107, 9415.
2. Hasegawa, M.; Negishi, Y. J Electrochem Soc 2005, 152, C221.
3. Kim, S.-K.; Josell, D.; Moffat, T. P. J Electrochem Soc 2006, 153, C616.
4. Rusli, E.; Xue, F. J Electrochem Soc 2007, 154, D584.
5. Li, X.; Drews, T. O. J Electrochem Soc 2007, 154, D230.
6. Hasegawa, M.; Okinaka, Y. Electrochem Solid State Lett 2006, 9, C138.
7. Drews, T. O.; Ganley, J. C. J Electrochem Soc 2003, 150, C325.
8. Tierno, P.; Goedel, W. A. J Phys Chem B 2006, 110, 3043.
9. Vereecken, P. M.; Binstead, R. A. IBM J Res Dev 2005, 49, 1.
10. Lattimer, R. P. J Anal Appl Pyrol 2001, 56, 61.
11. Voorhees, K. J.; Baugh, S. F.; Stevenson, D. N. Thermochim Acta 1996, 274, 187.
12. Gallet, G.; Carroccio, S.; Pizzarelli, P.; Karlsson, S. Polymer 2000, 43, 1081.
13. Hassouna, F.; Morlat-Therias, S.; Mailhot, G.; Gardette, J. L. Polym Degrad Stab 2007, 92, 2042.
14. Uchiyama, T.; Kiritoshi, Y.; Watanabe, J.; Ishihara, K. Biomaterials 2003, 24, 5183.
15. Chen, C. C.; Rajeshwar, K. J Electrochem Soc 1994, 141, 2942.
16. Kim, K.-W.; Lee, E.-H.; Kim, J.-S.; Shin, K.-H.; Jung, B.-I. Electrochim Acta 2002, 47, 2525.
17. Fukatsu, K.; Kokot, S. Polym Degrad Stab 2001, 72, 353.
18. Khatua, S.; Hsieh, Y.-L. J Polym Sci Part A: Polym Chem 1997, 35, 3263.
19. Epstein, J. A.; Lewin, M. Textil-Rundschau 1961, 16, 494.
20. Puglisi, C.; Samperi, F. Macromolecules 1999, 32, 8821.
21. Kawasaki, H.; Takeda, Y. Anal Chem 2007, 79, 4182.
22. Lattimer, R. P.; Polce, M. J. J Anal Appl Pyrol 1998, 48, 1.
23. Frisch, M. J.; Trucks, G. W.; Schlegel, H. B.; Scuseria, G. E.; Robb, M. A.; Cheeseman, J. R.; Montgomery, J. A., Jr.; Vreven, T.; Kudin, K. N.; Burant, J. C.; Millam, J. M.; Iyengar, S. S.; Tomasi, J.; Barone, V.; Mennucci, B.; Cossi, M.; Scalmani, G.; Rega, N.; Petersson, G. A.; Nakatsuji, H.; Hada, M.; Ehara, M.; Toyota, K.; Fukuda, R.; Hasegawa, J.; Ishida, M.; Nakajima, T.; Honda, Y.; Kitao, O.; Nakai, H.; Klene, M.; Li, X.; Knox, J. E.; Hratchian, H. P.; Cross, J. B.; Bakken, V.; Adamo, C.; Jaramillo, J.; Gomperts, R.; Stratmann, R. E.; Yazyev, O.; Austin, A. J.; Cammi, R.; Pomelli, C.; Ochterski, J. W.; Ayala, P. Y.; Morokuma, K.; Voth, G. A.; Salvador, P.;

Dannenberg, J. J.; Zakrzewski, V. G.; Dapprich, S.; Daniels, A. D.; Strain, M. C.; Farkas, O.; Malick, D. K.; Rabuck, A. D.; Raghavachari, K.; Foresman, J. B.; Ortiz, J. V.; Cui, Q.; Baboul, A. G.; Clifford, S.; Cioslowski, J.; Stefanov, B. B.; Liu, G.; Liashenko, A.; Piskorz, P.; Komaromi, I.; Martin, R. L.; Fox, D. J.; Keith, T.; Al-Laham, M. A.; Peng, C. Y.; Nanayakkara, A.; Challacombe, M.; Gill, P. M. W.; Johnson, B.; Chen, W.; Wong, M. W.; Gonzalez, C.; Pople, J. A. Gaussian 03, Revision C.02; Gaussian, Inc.: Wallingford,CT, 2004.

24. Becke, A. D. J Chem Phys 1993, 98, 1372.
25. Stephens, P. J.; Devlin, F. J.; Chabalowski, C. F.; Frisch, M. J. J Phys Chem 1994, 98, 11623.
26. Begum, R.; Matsuura, H. J Chem Soc Faraday Trans 1997, 93, 3839.
27. Oesterhelt, F.; Rief, M.; Gaub, H. E. New J Phys 1999, 1, 6.
28. Okamoto, Y. J Cryst Growth 1998, 191, 405.
29. Timoshkin, A. Y.; Bettinger, H. F.; Schaefer, H. F., III. Inorg Chem 2002, 41, 738.